

Bluff Body Aerodynamics and Flow Separation

Jeffrey Newcamp

Group 4

AME 342

18 September 2002

1 Abstract

A bluff body is one in which the length in the flow direction is close to or equal to the length perpendicular to the flow direction. This spawns a unique characteristic, namely, that skin friction drag is much lower than pressure drag. Therefore, measuring the aerodynamic forces on a bluff body is simplified. For this experiment, a circular cylinder was inserted into a viscous flow field using a subsonic wind tunnel. Pressure taps along the spanwise direction of the cylinder measured static pressure differences, whereas a free-stream pitot tube measured free-stream pressure. Manometers supplied data in the form of output voltages from each pressure setup. The flow over the cylinder generated aerodynamic forces, leading to pressure distribution, a wake and vortex shedding. The goals of the experiment were 1) to show the pressure distribution over the cylinder and to calculate the section lift and drag coefficients 2) to use wake velocity profile and the integral momentum conservation equation to determine drag and 3) to calculate the vortex shedding frequency for three Reynolds numbers (Iqbal 1). A detailed comparison and articulation of the experimental observations and data is made. Theoretical results and proven experimental data from other sources are included for thorough discussion of the bluff body aerodynamics. Two-dimensionality, steady flow and incompressibility are assumed at stages in the experiment. The goal of the report is to identify the characteristics of bluff body aerodynamics and to prove why airfoils are shaped as they are.

Table of Contents

Section	Page(s)
1. Abstract	2
Table of Contents	3
2. Nomenclature	4
3. Introduction	5-7
4. Experimental Apparatus and Procedure	8-10
5. Results and Discussion	11-16
6. Conclusions	17
7. References	18
8. Appendix	19-20

2 Nomenclature

Symbol	Description	Unit(s)
μ_{∞}	free-stream viscosity	slug / ft*s
π	pi	dimensionless
θ	angle of rotation of cylinder (opposing flow direction corresponds to $\theta = 0$)	radians
ρ	density	slugs / ft ³
C_d	drag coefficient	dimensionless
C_l	lift coefficient	dimensionless
C_p	pressure coefficient	dimensionless
d	diameter	inches
f_s	frequency	hertz
p_s	static pressure	lb / ft ² or (inches of water)
p_{∞}	free-stream pressure	lb / ft ² or (inches of water)
U_{∞}	free-stream velocity	ft / s
V_{∞}	free-stream velocity	ft / s
x	cylinder diameter	inches

3 Introduction

3.1 Background

For inviscid flow, there is no friction to cause boundary layer separation, vortices or a subsequent wake. However, inviscid flow over a cylinder will generate areas of different pressure gradients. Two stagnation points result – one on the middle of the cylinder in the fluid flow direction and one behind the cylinder. At these points, C_p will be one. Since the cylinder is a symmetric body, there will be symmetric pressure regions around the body. In the direction perpendicular to the fluid flow, a suction force exists. Again, since the body is symmetric, so are the forces – and therefore, the forces negate each other. In this inviscid scenario, no aerodynamic forces result because of the symmetry. The simplification that the flow is inviscid fails because bluff bodies experience aerodynamic forces. Theoretical equation (1) can merely be used as a benchmark for validating data.

$$C_p = 1 - 4 \sin^2 \theta \quad (1)$$

For the purpose of this experiment, the fluid flow was analyzed as viscous. Viscous flow over a circular cylinder does not separate, but viscous flow does separate, causing wake vortices and measurable wake pressure/velocity data. The pressure coefficient is governed by equation (2).

$$C_p = \frac{(p_s - p_\infty)}{\rho U_\infty^2 / 2} \quad (2)$$

Whereas p_s is the static pressure and p_∞ is free-stream pressure, both measured using a pitot-static system attached to a manometer. The reference velocity (free-stream) is denoted by U_∞ . Using pressure coefficient data and knowing the measurement locations on the cylinder, one can calculate drag (equation 3)) and lift around the cylinder using numerical integration.

$$C_d = \frac{D'}{\rho U_\infty^2 d / 2} \quad (3)$$

Equation (4) shows a proper summation of drag forces around the cylinder to produce the drag coefficient. Replacing (cos) with (sin) yields the lift force coefficient (Thomas Lecture).

$$C_d = \frac{1}{2} \sum_{n=1}^N C_{pi} \cos \theta_i \Delta \theta_i$$

(4)

Integral momentum analysis can also be used to find the drag coefficient. See “Drag Estimate via Integral Momentum Analysis” by Flint Thomas. For viscous flow, friction exists at the boundary of any bluff body (shear stress is not zero). Flow near body surfaces slows down, an adverse pressure gradient (equation (5)) develops and a boundary layer will separate.

$$\frac{dP}{ds} > 0$$

(5)

Where ds is the distance traveled over a body. Once flow separates, as seen in Figure A in Appendix 1, vortex shedding results. It has a frequency, is related to the free-stream velocity and consequently changes as the Reynolds number changes (equation (6)).

$$\text{Re} = \frac{\rho V_{\infty} x}{\mu_{\infty}}$$

(6)

Vortices from the top and bottom of the cylinder are shed, causing two rows of vortices downstream. Such a phenomenon causes unsteady forces on the cylinder and can, in extreme cases, cause structural failure. The time scale for flow over a cylinder is found by taking the diameter of the cylinder and dividing by the free-stream velocity. Also, calculating the time scale for the shedding frequency and taking its reciprocal yields the shedding frequency. Taking a ratio of the two time scales yields the Strouhal number, shown in equation (7).

$$\text{St} = \frac{f_s d}{U_{\infty}}$$

(7)

Knowing pressure distributions, drag, Reynolds numbers, shedding frequencies and Strouhal numbers will lead to a full analysis of this experiment and the implications therein.

3.2 Objectives

The experiment seeks to help one gain understanding of several aerodynamic phenomenon. First is pressure distribution around a circular cylinder. By using static pressure measurements obtained from pressure taps along the spanwise direction of the cylinder, as well as free-stream pressure measurements, pressure distribution can be plotted. Stagnation points, areas of suction and the location of separation can be pinpointed. Lastly, lift and drag coefficients can be calculated using the pressure data and numerical integration. Running the wind tunnel at different speeds for this part of the experiment yields data for several Reynolds numbers.

The second part of the experiment involved plotting the wake profile behind the circular cylinder at one Reynolds number. A pitot tube was mounted on a rod, connected to a small motor. Starting behind the circular cylinder in reference to the fluid flow, measurements were taken from the center of the cylinder to a location near the top of the wind tunnel. The data can show the wake as well as the location where the streamlines are no longer affected by the bluff body. Measurements traversing the wake yield data corresponding to wake width and velocity defect.

Vortex shedding is discussed in the third experiment. A hot-wire probe is inserted into the test section behind the cylinder and it takes voltage measurements for a free stream velocity in a range from 5 m/s to 15 m/s. When plotted, using a fourier transform technique, the voltage values are set against a time scale and spikes on the plot evidence the periodicity of the flow. Each spike represents a cooling due to flow over the hot-wire, thus indicating one vortex.

The remainder of the report will be organized into sections, 4) Experimental Apparatus and Procedure, 5) Results and Discussion, 6) Conclusions, 7) References and 8) Appendix. Data will be analyzed in the results section. Graphical results and tables will be presented, as will accompanying uncertainty analysis. Experimental conclusions will be presented in the conclusions section. The three subparts of the experiment will be related and discussed in terms of final conclusions. Popular questions like, "What does all of this data mean," will be answered.

4 Experimental Apparatus and Procedure

A wind tunnel setup was needed for this experiment. A diagram is shown in Appendix 1, Figure B. The wind tunnel chosen was a subsonic tunnel due to the low-speed needs for this experiment. The tunnel test section is large enough to avoid significant wall effects. A circular cylinder with diameter of 1.65 ± 0.005 inches was placed into the test section, set on a rotating rod. Additionally, a pitot-static setup was placed near the inlet to the tunnel to measure free-stream pressure. A pitot tube on a traverse mechanism and a hot wire were both placed behind the circular cylinder. The traverse mechanism was run by a computer application (Traverse.vi) that moved the measuring device 5 mm for every 4000 steps (0.2 inches per 4000 steps). Appendix 1, Figure C shows the test section of the wind tunnel. It gives detail of the circular cylinder placed into the flow field. Of interest, there are several pressure taps located spanwise on the cylinder. Each can be measured using a manometer to yield pressure changes. Two manometers were used in the experiment, each with different calibration factors. The first manometer measured the free-stream velocity, using the total pressure port and the static pressure port. For the free-stream manometer, the calibration equation is shown as equation (8).

$$(voltage * 1.013524 - 0.0043) \tag{8}$$

The second manometer measured p_∞ and static pressure from a cylinder surface pressure tap. The calibration constant is shown as equation (9).

$$(voltage * 1.1072) \tag{9}$$

The calibration for each manometer gives a value in inches of water. That must be converted to be used in most standard equations. Note: Calibration equations will be different for every manometer. To find velocity using inches of water, equation (10) was used.

$$V_\infty = \sqrt{\frac{2 * 9.81 * 25.4 * (\text{inches_of_water})}{1.2}} \tag{10}$$

1) By rotating the cylinder through a range of angles, pressure measurements can be taken around the cylinder. Such information provides information on boundary layer separation and aerodynamic forces. The computer program, Data.vi, recorded the pressure distribution data.

2) The pitot tube behind the cylinder used to traverse the wake had a dynamic pressure port (total pressure), but no static port. The total pressure was connected to a manometer, as was a reference pressure denoted by p_∞ . The computer program, *Traverse.vi*, recorded the wake data.

3) The hot-wire (Auspex type) anemometer system worked independent of the manometers. A hot-wire is a thin wire that cools when in a flow. The change in temperature is sensed as voltage and can be converted into velocity or used as a voltage-time series to plot the frequency of the vortex shedding. The computer program, *Spectrum.vi*, recorded the hot-wire data signal.

4.1 Pressure Distribution

The voltmeter was zeroed, and the tunnel was run up to 10 m/s to calibrate the manometer to a reading of '1.' The cylinder was rotated in increments of 5 ± 0.5 degrees (0.08727 ± 0.008727 radians) through 360 degrees, beginning with the pressure taps directly opposed to the flow direction. Recording the manometer readings for static cylinder and free-stream pressures ($p_s - p_\infty$) can generate a plot of pressure regions around the cylinder. The experiment was repeated for three different speeds, 9.962 ± 0.011 m/s, 11.157 ± 0.011 m/s and 15.156 ± 0.009 m/s.

4.2 Wake Survey

The pitot tube behind the cylinder recorded the pressure ($P - p_\infty$) at each vertical position. To begin, the voltmeter was adjusted to zero and the tunnel was run at 0.34 ± 0.005 volts, or a speed of 11.888 ± 0.010 m/s (found using equations (8) and (10)). The traverse mechanism was run from the center of the cylinder to near the top of the wind tunnel. The traverse was taken to the top to ensure valid data outside of the wake, where no pressure gradient exists and the measurements remain constant.

4.3 Vortex Shedding

Hot-wire data was acquired by placing the hot-wire device in line with the edge of the cylinder and at the center line of the cylinder. Connections for the hot-wire were made and the wind tunnel was turned on. Measurements were taken at the five voltages/velocities shown in Table (4.1).

Voltage (V ± 0.005)	Velocity (m/s)
0.07	5.260 ± 0.015
0.15	7.833 ± 0.013
0.25	10.171 ± 0.011
0.39	12.742 ± 0.010
0.46	13.850 ± 0.010

Table (4.1)

The voltage-time series from the hot-wire anemometer were measured at both the edge and at the center line of the cylinder.

5 Results and Discussion

Reynolds number for all three parts of the experiment are shown in Table (5.1).

Subpart	Velocity (m/s)	Reynolds Number
Pressure Distribution	9.962 \pm 0.011	25871
Pressure Distribution	11.157 \pm 0.011	28976
Pressure Distribution	15.156 \pm 0.009	39362
Wake Survey	11.888 \pm 0.010	30874
Vortex Shedding	5.260 \pm 0.015	13663
Vortex Shedding	7.833 \pm 0.013	20342
Vortex Shedding	10.171 \pm 0.011	26414
Vortex Shedding	12.742 \pm 0.010	33093
Vortex Shedding	13.850 \pm 0.010	35970

Table (5.1)

Due to the relatively low Reynolds numbers, less turbulence results than at higher Reynolds numbers.

This is true because skin friction is a direct function of Reynolds number. According to published results, boundary layers transition to turbulent at or near Reynolds numbers of 10^5 . For this experiment, Reynolds number is directly related to fluid flow velocity, and will dictate the location of fluid flow separation from the bluff body. This information is applicable to real-life aerodynamics in that turbulence has higher skin friction drag, but laminar airfoils stall earlier.

5.1 Pressure Distribution

A simple test was conducted to ensure two-dimensionality of the flow, thus validating the assumption that flow is even across any spanwise location on the cylinder. At a constant free-stream velocity, pressure was measured along three different pressure taps at a constant cylinder rotation angle. The static pressure values are essentially the same at the three different locations, confirming the two-dimensionality theory. The resultant data is provided in Table (5.1.1).

Free-stream Pressure (volts)	Static Pressure (volts)
0.271016 \pm 5e-7	0.269922 \pm 5e-7
0.273018 \pm 5e-7	0.268574 \pm 5e-7
0.272578 \pm 5e-7	0.275625 \pm 5e-7

Table (5.1.1)

Pressure distribution around the cylinder (equation (2)) is plotted against the theoretical calculation for inviscid flow (equation (1)) at 11.157 m/s in Figure 5.1. Plots for 9.9615 m/s and 15.1563 m/s are similar in shape.

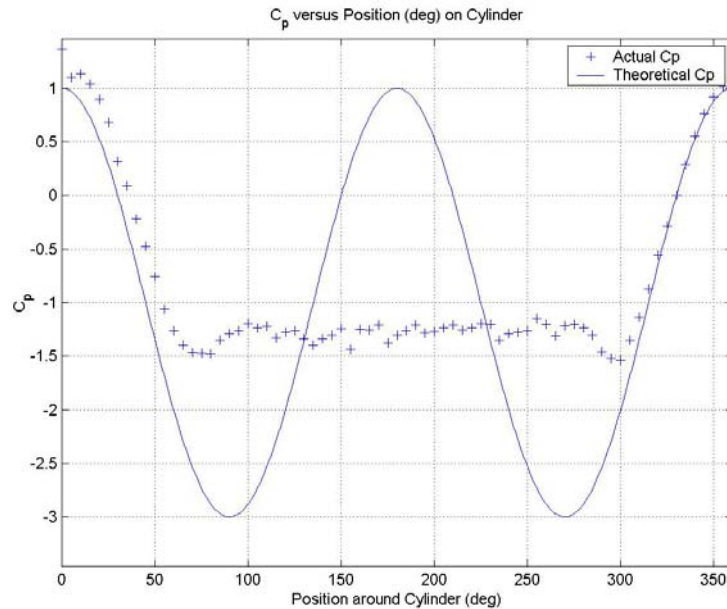


Figure 5.1.1

Figure 5.1 clearly shows separation from the cylinder before 100 degrees and reattachment by 300 degrees. Exact measures are expected to be 180 degrees apart due to the symmetry of the body. The points of separation on the top and bottom surfaces of the cylinder are where the pressure coefficient becomes unsteady. Additionally, C_p approaches the value of one at the two stagnation points, 0 degrees and 360 degrees, or the front and rear midpoints of the cylinder. When plotted for higher Reynolds numbers, the stagnation point moves forward and pressure increases at the surface of the cylinder behind the oncoming flow. This results in less drag force on the cylinder.

5.2 Wake Survey

The wake was surveyed at 11.888 ± 0.010 m/s (39.003 ± 0.033 ft/s) from the center of the cylinder to the top of the wind tunnel test section. Figure 5.2.1 accurately shows that far above the cylinder, free-stream velocity is measured by the pitot tube. However, in the wake behind the cylinder, velocity is greatly reduced.

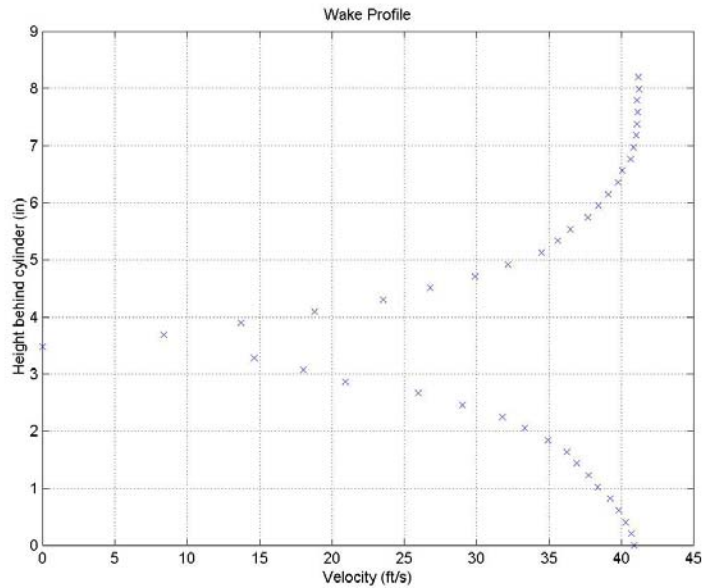


Figure 5.2.1

Velocity defect at different Reynolds numbers is quite noticeable. As the Reynolds number increases, a turbulent boundary layer develops. Due to the pressure gradient, the boundary layer remains on the cylinder longer than if the Reynolds number were lower. Therefore, at higher Reynolds numbers, the wake width becomes smaller. Consequently, the velocity defect decreases (Drag of Blunt). Using two different methods to compute the drag coefficient, the experimental results are shown in Table 5.2.1.

Subpart	Method	Velocity (m/s)	Drag coefficient (C_d)	Lift coefficient (C_l)	Reynolds Number
Pressure Distribution	Numerical Integration	9.962 ± 0.011	1.2382 ± 0.004	$0.0823 \pm 5e-4$	25871
Pressure Distribution	Numerical Integration	11.157 ± 0.011	1.1705 ± 0.004	$0.0483 \pm 4e-4$	28976
Pressure Distribution	Numerical Integration	15.156 ± 0.009	1.1500 ± 0.003	$0.0566 \pm 5e-4$	39362
Wake Survey	Integral Momentum Analysis	11.888 ± 0.010	1.0347 ± 0.004	-	30874

Table (5.2.1)

Appendix 1, Figure D shows a plot of the drag coefficient versus the Reynolds number for a circular cylinder (Kuethe 439). Note how drag rapidly increases at low Reynolds numbers. For the bluff body experiment, the Reynolds numbers were relatively low. The high and low ends of the plot are not of particular interest. However, note the general relation between Re and C_D . At Reynolds numbers between

20,000 and 30,000, experimental results indicate the drag coefficient should be near 1.2. Therefore, this experiment is within range.

Numerical integration used the pressure distribution data around the cylinder. The drag coefficient was calculated using equation (4). The purpose of that equation is to perform the Trapezoidal Rule. The summation of the bits of drag around the cylinder, some positive and some negative, generates the total drag around the cylinder (Calculation of C_d Lecture). Pressure data was taken at three free-stream velocities, therefore, there are three drag and lift calculations for the three different Reynolds numbers.

Integral momentum analysis was the second method utilized to calculate the drag coefficient for the cylinder. The wake velocity profile data was used for this calculation. Summing the momentum in and the momentum out determines the total drag experienced. The drag value is then used to determine the drag coefficient using equation (3). The full momentum derivation is contained in the handout, "Drag Estimate via Integral Momentum Analysis" by Flint Thomas.

5.3 Vortex Shedding

The hot-wire data was acquired for five wind tunnel speeds and subsequent voltage-time series were plotted at both the edge and the center line of the cylinder. The MatLab command for Fourier transform was used to determine the cylinder shedding frequency. The data appeared as a series of spikes along the horizontal axis. The largest spike in each graph (corresponding to each of five wind tunnel speeds) aligned with the shedding frequency. In order to sum the spikes more readily, a resolution of 256 points was used as opposed to 512 points or greater. Figure 5.3.1 shows an example of the data output from hotwire1.m. The data for this plot was taken at the edge of the cylinder, therefore, only one set of vortices was sensed by the hotwire.

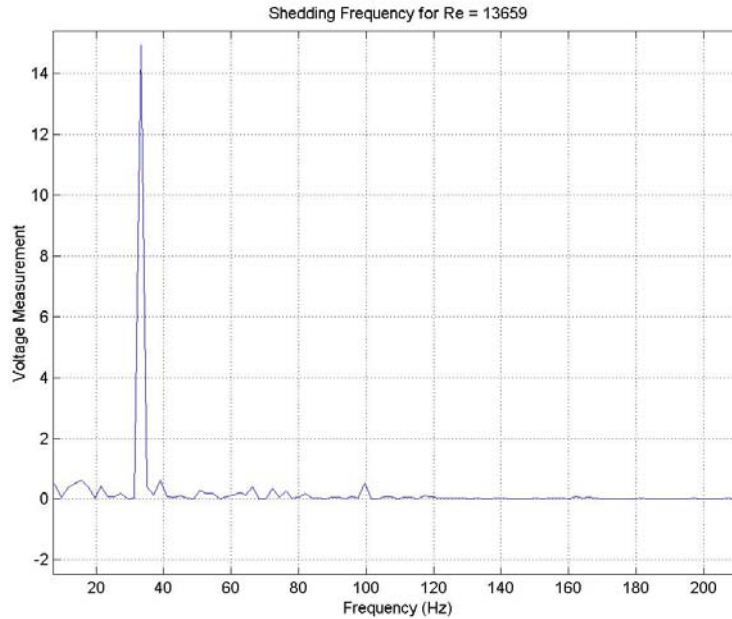


Figure 5.3.1

A fairly pronounced spike at frequency equal to 33 ± 0.5 Hz shows the shedding frequency for this particular Reynolds number. As a note, frequencies over time were averaged to provide one more accurate measurement per Reynolds number. Data with low frequency (10-20 Hz) was erroneous due to wall effects, so that data was ignored. Data taken at the center of the cylinder reflects how two sets of alternating vortices could be sensed by the hotwire. Therefore, the frequency of the vortex shedding is nearly double for the center measurements, as seen in Figure 5.3.4.

Figure 5.3.2 plots frequency versus Reynolds number for the edge measurements. Figure 5.3.3 plots Strouhal number (equation (7)) versus Reynolds number (equation(6)) for the edge measurements.

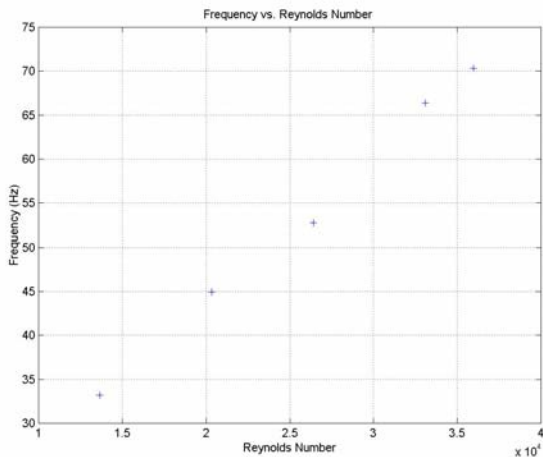


Figure 5.3.2

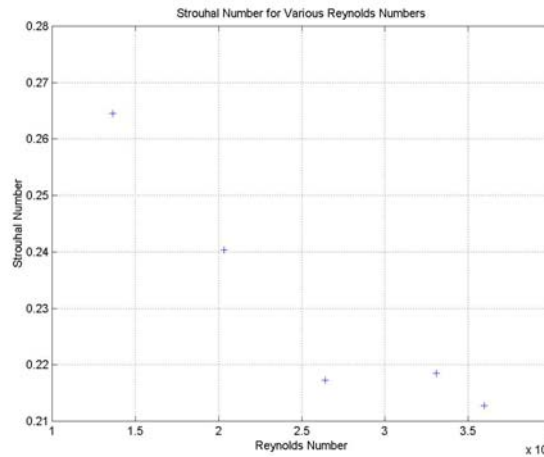


Figure 5.3.3

Figure 5.3.4 plots frequency versus Reynolds number for the center measurements. Figure 5.3.5 plots Strouhal number versus Reynolds number for the center measurements.

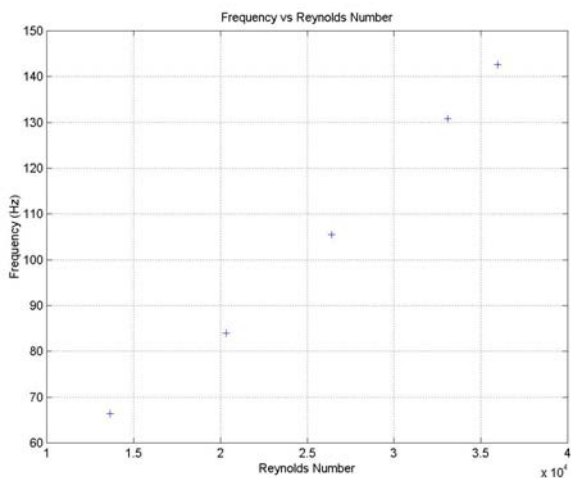


Figure 5.3.4

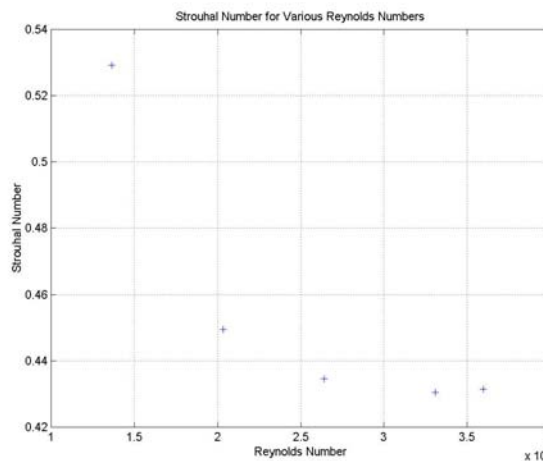


Figure 5.3.5

Figures 5.3.2 and 5.3.4 show that increasing Reynolds numbers yield increasing shedding frequencies (as a nearly linear relationship). Published data suggests that the Strouhal number for Reynolds numbers near 10^4 should center near 0.21 (Flow). This experiment's data is fairly coincident with the published data, except for one seemingly erroneous Strouhal number at the lowest recorded Reynolds number.

6 Conclusions

This experiment aided student comprehension of many common aerodynamic phenomenon. Bluff bodies are a unique series of geometries in terms of flow dynamics. The circular cylinder used in this experiment, and other bluff bodies, have flow separation due to pressure gradients. Separation causes pressure drag and therefore reduces the effectiveness of the body for producing lift. By stretching the bluff body, such as adding a fairing to the backside of a circular cylinder, the flow over the body changes. The adverse pressure gradient reduces as the body becomes more streamlined. Therefore, drag is also reduced. By making the body asymmetric, forces are generated that can be used in modern aerospace applications. This experiment showed how the pressure distribution and drag act around a bluff body. Additionally, the experiment proved theory concerning the boundary layer, Reynolds numbers, Strouhal numbers, wake profile and shedding frequency of a bluff body. Converting a bluff body to an airfoil does all but eliminate the aforementioned phenomenon. Whereas shedding frequencies can sometimes be harmful to aerospace applications, Reynolds numbers and boundary layers can be used to design more efficient airfoil geometries. This proves that bluff body aerodynamics are helpful in understanding more complicated airfoil aerodynamics.

7 References

- “Drag of Blunt Bodies and Streamlined Bodies.” [Internet].
http://www.princeton.edu/~asmits/Bicycle_web/blunt.html. Princeton University.
- “Flow visualization: flow around a cylinder at Reynolds number 40 - 200.” [Internet].
<http://www.cwr.uwa.edu.au/cwr/teaching/flowvis/flowvis.htm>. Center for Water Research.
- Iqbal, Muhammad O. and Sergio Escobar-Vargas. “Experiment 1: Bluff Body Aerodynamics.” Handout. University of Notre Dame, 3 September 2002.
- Kuethe, Arnold M. and Chuen-Yen Chow. Foundations of Aerodynamics: Bases of Aerodynamic Design. New York: John Wiley & Sons, Inc, 1998.
- Thomas, Flint. Lecture. “Calculation of C_d for Circular Cylinder.” University of Notre Dame, 13 Sept. 2002.
- Thomas, Flint. “Drag Estimate via Integral Momentum Analysis.” Handout. University of Notre Dame, 4 Sept. 2002.

8 Appendix 1

Setup Figures and Flow

Figure A) Viscous Flow Over a Circular Cylinder (Iqbal)

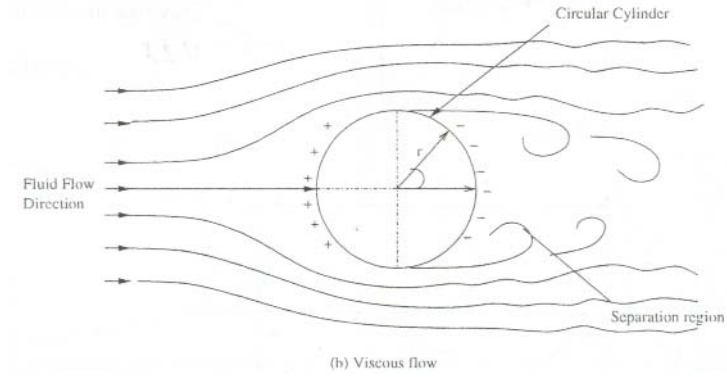


Figure B) Apparatus and Wind Tunnel (Iqbal)

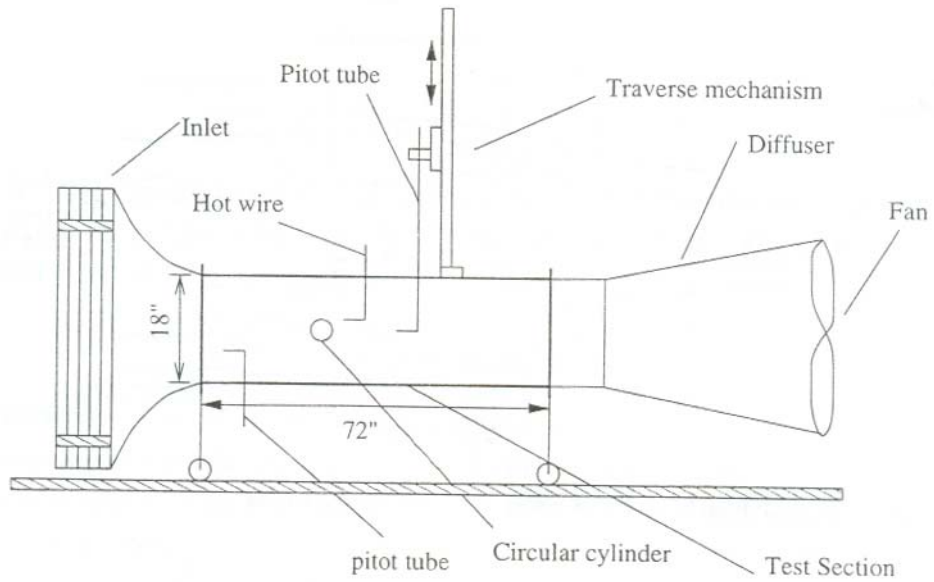


Figure C) Cylinder Setup, Pressure Taps, Hot Wire Setup, Wake Survey Setup (Iqbal)

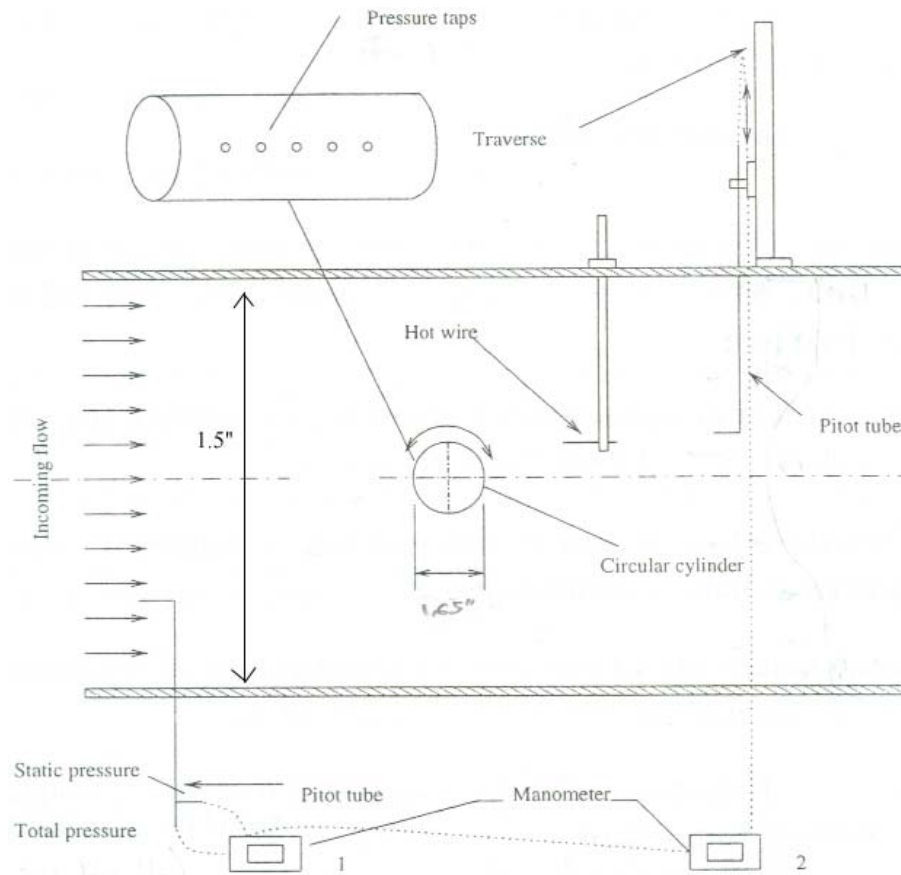


Figure D) Measured drag coefficient for a circular cylinder as a function of Reynolds Number (Kuethe)

